Valley Subband Splitting in Bilayer Graphene Quantum Point Contacts

R. Kraft,[1] I. V. Krainov,[2,5] V. Gall,[1,3] A. P. Dmitriev,[2] R. Krupke,[1,4] I. V. Gornyi,[1,2,3] and R. Danneau[1,*]
[1]Institute of Nanotechnology, Karlsruhe Institute of Technology, D-76021 Karlsruhe, Germany
[2]A.F. Ioffe Physico-Technical Institute, 194021 St. Petersburg, Russia
[3]Institute for Condensed Matter Theory, Karlsruhe Institute of Technology, D-76128 Karlsruhe, Germany
[4]Department of Materials and Earth Sciences, Technical University Darmstadt, 64287 Darmstadt, Germany
[5]Lappeenranta University of Technology, P.O. Box 20, 53851 Lappeenranta, Finland

(Received 17 September 2018; published 20 December 2018)

We report a study of one-dimensional subband splitting in a bilayer graphene quantum point contact in which quantized conductance in steps of $4e^2/h$ is clearly defined down to the lowest subband. While our source-drain bias spectroscopy measurements reveal an unconventional confinement, we observe a full lifting of the valley degeneracy at high magnetic fields perpendicular to the bilayer graphene plane for the first two lowest subbands where confinement and Coulomb interactions are the strongest and a peculiar merging or mixing of K and K' valleys from two nonadjacent subbands with indices $(N, N+2)$, which are well described by our semiphenomenological model.

DOI: 10.1103/PhysRevLett.121.257703

Thirty years after its discovery, quantized conductance resulting from the discretization of the one-dimensional (1D) subbands in a ballistic constriction remains one of the most striking effects in mesoscopic physics [1–5]. Thanks to the rapid development of nanofabrication, the quantum point contact (QPC) geometry [6] used in these experiments has become a basic tool to study 1D physics [7] and design complex devices and circuits, as it can act as a beam splitter in electron opticslike experiments [8–10], as well as noninvasive charge detectors [11–16]. While a vast majority of 1D ballistic systems shows quantized conductance in units of $2e^2/h$, where the factor of 2 is due to spin degeneracy, only few involve an additional valley degree of freedom such as Si-SiGe heterostructures [17–21], AlAs quantum wells [22], carbon nanotubes [23] or single-layer and bilayer graphene (SLG and BLG) [24–35]. Spin and valley degeneracy should give rise to conductance steps of $4e^2/h$. However, deviations from this expected quantized value have been typically observed [17–28,33–35], and usually explained by the lifting of the valley degeneracy because of confinement.

Controlling the valley isospin and breaking the valley degeneracy appears to be crucial in the development of valleytronics [36]. Valley degeneracy could be tuned for various conditions and geometries [37–40]; in graphene, the design of valley filters and valley valves has been proposed based on ballistic QPCs [41]. In addition, lifting the valley degeneracy appears to be essential in graphene spin qubits [42]. Here, we present experiments on ballistic transport through a QPC electrostatically defined in BLG. To study the nontrivial splitting of the 1D subbands in this fourfold degenerate system, we have employed local band-gap engineering [43], source-drain bias spectroscopy [44–46], magnetoelectric subband-depopulation technique [47,48], and semiphenomenological modeling. At lowest magnetic fields, quantization of the QPC conductance in units of $4e^2/h$ is clearly observed. With increasing magnetic field, these steps split, forming a peculiar pattern combining steps of e^2/h, $2e^2/h$, and $4e^2/h$. Our model, based on the 2×2 Hamiltonian [49,50], agrees well with the full splitting of the Landau levels for the lowest two channels, as well as with the observed exotic merging or mixing of the K and K' valleys from pairs of 1D subbands with $(N, N+2)$ indices.

For this study, we have used a device on which 1D confinement without edge currents was induced by local band-gap engineering and characterized by proximity-induced superconductivity and magnetointerferometry [43]. In those experiments, we used the displacement field created by the back gate and split gate (BG and SG) to locally open a band gap and confine the charge carriers in the QPC. However, keeping this geometry does not allow us to drive the constriction to the low-density regime and observe the quantized conductance. In order to reach this regime, here we have added an overall top gate (TG) on an edge-connected BLG encapsulated between a bottom and top hexagonal boron nitride (hBN) multilayers, as depicted in Fig. 1 (see Ref. [43] and Supplemental Material [51] for details on the sample fabrication). As the BG counteracts and dominates over the SG for the control of the carrier density within the constriction, we use the TG to control the density not only by tuning the Fermi level [55–57] but also by opening a band gap in the 2D reservoirs and the constriction via the displacement field induced by BG and TG. Therefore, while keeping BG and SG voltages constant, sweeping the TG voltage tunes the Fermi level, the

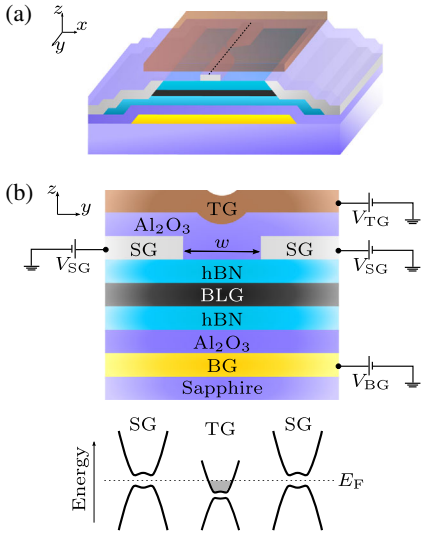

FIG. 1. (a) Schematic illustrating the device layout. (b) Cross section of the device along the dashed line in (a), together with a sketch of the electronic band structure across the constriction defined by the SG.

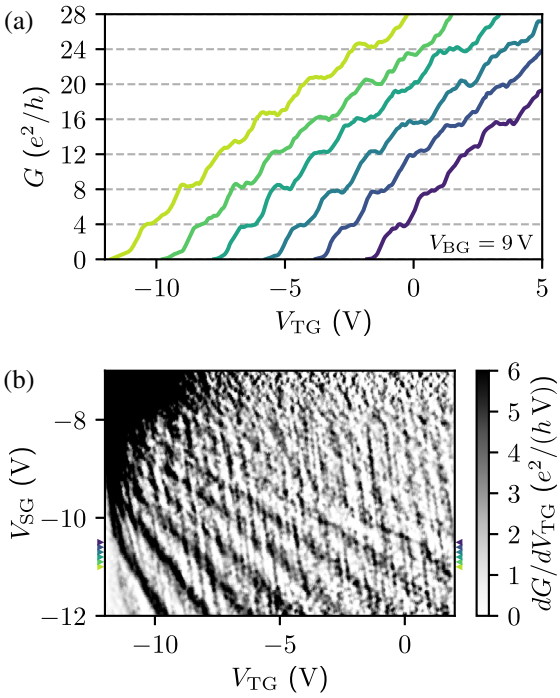

FIG. 2. (a) Differential conductance G as a function of V_{TG} for different values of V_{SG} from -11.0 (left) to -10.5 V (right) with an increment of 0.1 V and at constant $V_{BG} = 9$ V. The curves are shifted for clarity by 2 V between consecutive traces (the leftmost curve is not shifted). Well-quantized plateaus are observed in steps of $4e^2/h$. (b) Gray scale map of dG/dV_{TG} as a function of V_{TG} and V_{SG} at $V_{BG} = 9$ V. Small markers denote the position of line cuts shown in (a).

confinement, and the band structure in the induced 1D system, down to full pinch-off [51]. A small perpendicular magnetic field $B = 20$ mT was applied to keep the Al leads in the normal metal state.

In Fig. 2(a), the differential conductance G through the QPC as a function of TG voltage V_{TG} is displayed for different SG voltages V_{SG} at a constant BG voltage $V_{BG} = 9$ V. The conductance curves are shifted for clarity and are based on raw data with no series resistance subtracted [58]. A robust and stable quantized staircase in G is observed with plateaus at integer values of $4e^2/h$ (see the Supplemental Material [51] for more details on the stability of the plateaus). We note that quantization of conductance appears only in a limited range of V_{SG} for a given V_{BG}, when the Fermi level underneath the SG is placed in the induced band gap. In Fig. 2(b), a gray scale map of the differentiated differential conductance dG/dV_{TG} as a function of both V_{TG} and V_{SG} over an extended range of V_{SG} is displayed. The small colored triangles mark the V_{SG} values of the corresponding conductance traces shown in Fig. 2(a). The respective quantized plateaus are visible as large stripes that are tuned by both TG and SG. The plateaus, white in the gray scale map, are spreading with increasing V_{SG} that corresponds to an increasing subband level spacing as the confinement strengthened. The continuous evolution of the plateaus highlights the stability of the electrostatic confinement.

It is important to note that no signs of anomalous features below the first quantized plateaus, namely, the 0.7 structures [59,60], can be seen at the very low temperature of the experiment, $T \sim 20$ mK. One can also note that, within the plateaus in Fig. 2(a), additional faint oscillations are observed. Superimposed on the oblique large stripes corresponding to the quantized plateaus, the additional oscillations appear as more faint vertical lines in Fig. 2(b), mainly tuned by V_{TG} but almost independent of V_{SG}. We attribute these oscillations to Fabry-Pérot interferences arising from the two cavities formed by the contacts and the SG-induced barriers. We estimate the associated cavity size from the frequency of the resonances, yielding a length of about 230 nm, which is in good agreement with the device geometry [51]. Strikingly, two phenomena that are both directly linked to the ballistic nature of the charge carrier transport but having two different physical origins, are visible concurrently.

In order to characterize the 1D confinement of charge carriers and extract the subband spacing $\Delta E_{N,N+1}$, we have performed source-drain bias spectroscopy [44–46]. Figure 3(a) shows the transconductance dG/dV_{TG} as a function of source-drain bias voltage V_{bias} and V_{TG}. Here, the plateaus appear in black, while colored lines represent transitions between the plateaus, i.e., the subband edges. Subband edge crossings are marked by small crosses and $\Delta E_{N,N+1}$ increases approximatively linearly from about 4 to 9 meV for the first to the eighth subband. We note that this differs significantly from what is usually observed in QPCs, where one can model the system by a parabolic

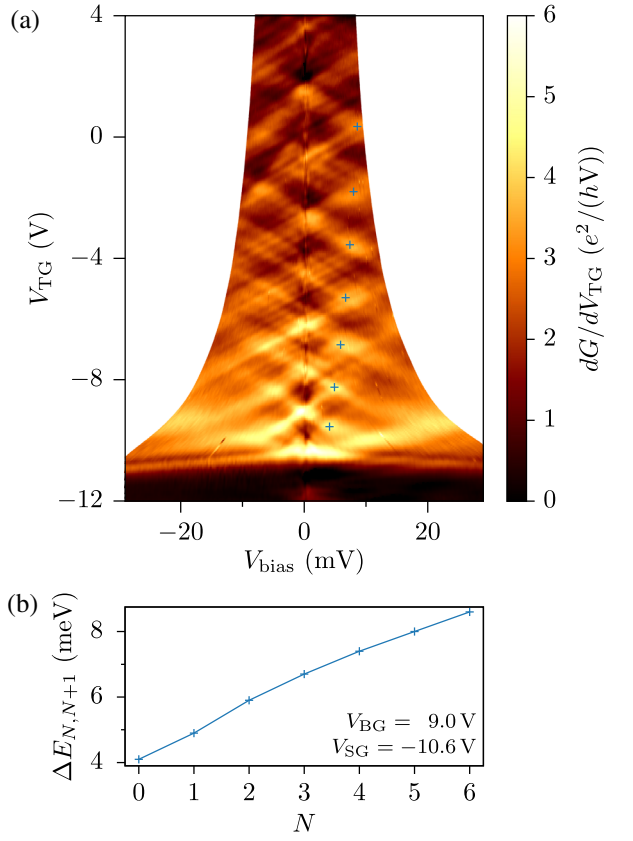

FIG. 3. (a) Transconductance versus source-drain bias voltage V_{bias} and V_{TG}. Minima in dG/dV_{TG} correspond to plateaus in the $G(V_{TG})$ curves. The resulting checkerboard pattern reveals an increasing energy level spacing with increasing subband index. Effect of the Fabry-Pérot interferences is clearly visible as lines parallel to the 1D subband dispersion lines. Blue crosses highlight the subband edge crossings representing the energy spacing $\Delta E_{N,N+1}$ between two consecutive 1D subbands of the QPC. (b) $\Delta E_{N,N+1}$ showing a linear dependence as a function of the 1D subband indices N.

potential with $\Delta E_{N,N+1}$ increasing in the reversed fashion as the confinement is strengthened for lower subbands. Our system turns out to be more complex as the displacement field generated by the TG tunes the band structure within the 1D constriction. This makes the confinement in our QPC very challenging to model. In addition, we observe sets of lines parallel to the subband edge lines which can be attributed to the Fabry-Pérot interferences as aforementioned.

To further analyze our QPC, we have studied the evolution of the 1D subband edges under a magnetic field B perpendicular to the BLG plane. Figure 4(a) shows G as a function of V_{TG} for different B from 20 mT (black thick curve) to 8 T (red curve), from left to right in steps of 100 mT, at $V_{BG} = 9$ V and $V_{SG} = -10.6$ V. The curves are shifted for clarity by an offset of 200 mV between consecutive curves. A clear change in the quantization of the conductance steps is observed as B increases, from $4e^2/h$ to e^2/h suggesting full lifting of the 1D subband degeneracy at high B. Note that the full splitting of the 1D subbands is fully ambipolar; therefore it occurs for both holes and electrons [51]. While the full lifting of the degeneracy has been observed in the quantum Hall regime in SLG [61] and BLG [33], the transition from full degeneracy to full splitting has not been studied, to our knowledge. Figure 4(b) displays the transconductance as a function of B and V_{TG} of the data set of Fig. 4(a). This allows us to follow the complex 1D subband edge splitting of our QPC. Clear splitting of the 1D subbands, seen as dark lines in the gray scale map (bright parts represent quantized plateaus), is observed for the two first subbands (four lines each). However, splitting appears to be different at high B for the higher subbands. The combination of electric and magnetic fields results into a complex splitting and bunching of the so-called magnetoelectric subbands [47].

In order to understand deeper the complex subband splitting on a qualitative level, we have developed a semiphenomenological model [51] derived from the 2×2 Hamiltonian of BLG [49]. We ignore, for simplicity, the modification of the spectrum near the bottom of the conductance band and the top of the valence band (Mexican-hat and trigonal-warping features; for the analysis of their effect on the QPC conductance, see Ref. [40]). With increasing magnetic field, the evolution of the eigenenergies and eigenstates for the K and K' valleys (neglecting the spin splitting) can be expressed as follows:

$$E_N^K = \sqrt{\Delta^2 + (E_N^0)^2} \underset{B\to\infty}{\to} \sqrt{\Delta^2 + \omega_B^2 (N+1)(N+2)},$$
$$\Psi_K = \begin{pmatrix} \varphi_N \\ \frac{\hat{p}_+^2}{2m(E+\Delta)}\varphi_N \end{pmatrix} \underset{B\to\infty}{\to} \begin{pmatrix} \tilde{\varphi}_N \\ \tilde{\varphi}_{N+2} \end{pmatrix}, \quad (1)$$

$$E_N^{K'} = \sqrt{\Delta^2 + (E_N^0)^2} \underset{B\to\infty}{\to} \sqrt{\Delta^2 + \omega_B^2 (N-1)N},$$
$$\Psi_{K'} = \begin{pmatrix} \varphi_N \\ \frac{\hat{p}_-^2}{2m(E+\Delta)}\varphi_N \end{pmatrix} \underset{B\to\infty}{\to} \begin{pmatrix} \tilde{\varphi}_N \\ \tilde{\varphi}_{N-2} \end{pmatrix}. \quad (2)$$

Here E_N^0 denotes the size-quantization levels in the QPC at $B = 0$. The magnetic field, characterized by the cyclotron frequency ω_B, is included through the shift in momentum operators $\hat{p}_\pm = \hat{p}_x - eA_x/c \pm (i\hat{p}_y - ieA_y/c)$ by the corresponding vector potential.

At $B = 0$, the energy levels are degenerate in K and K' valleys. The components of the spinors are given by the electron wave functions of a 1D quantum well: φ_N ($N = 0, 1, 2, \ldots$). With increasing B, the size-quantization wave function trends to a harmonic-oscillator wave function with the same number $\varphi_N \to_{B\to\infty} \tilde{\varphi}_N$. This results in degenerate Landau levels in strong B for the valleys K and K' coming from two different subbands with indices N differing by 2, as shown in Eqs. (1) and (2). Figure 4(c)

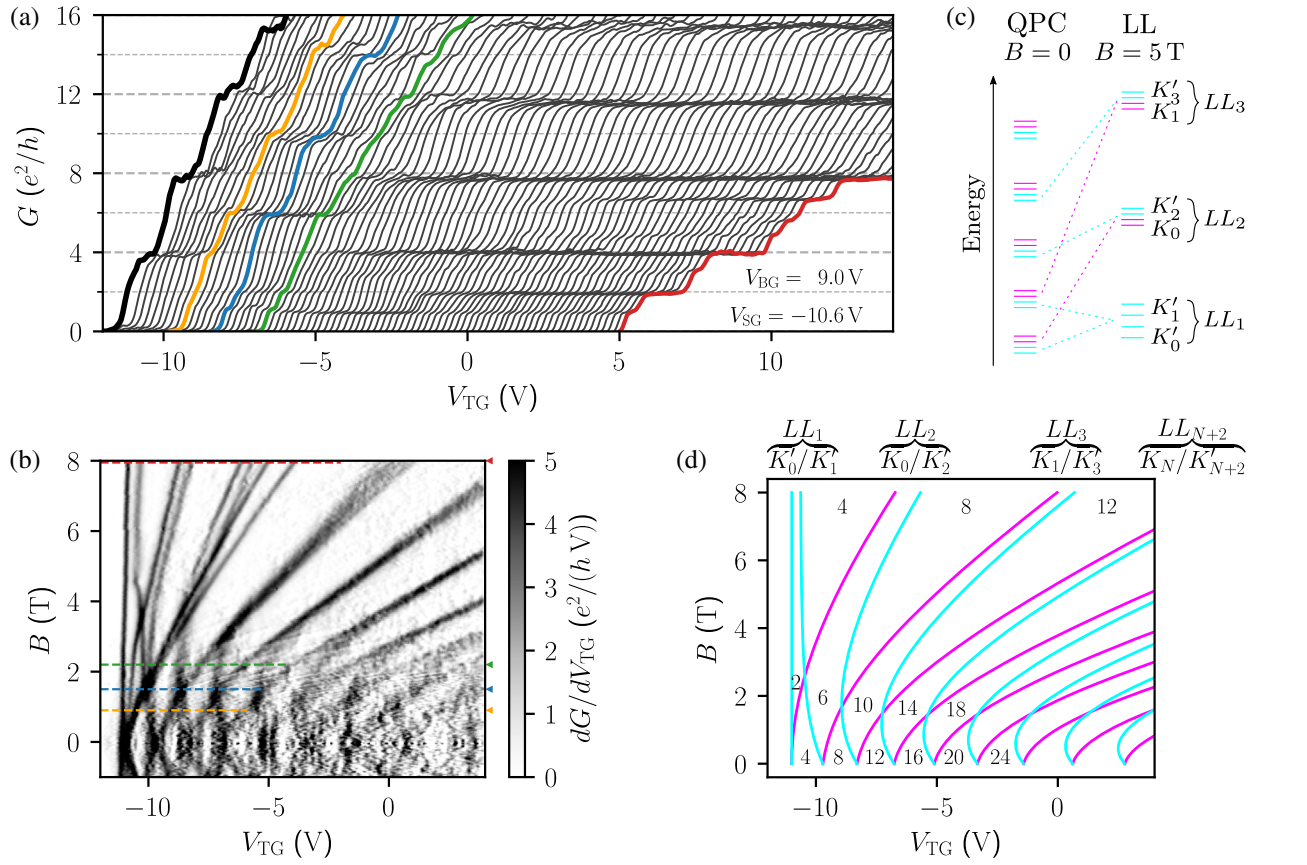

FIG. 4. (a) Differential conductance G as a function of V_{TG} for different values of magnetic field B in steps of 100 mT at fixed $V_{\mathrm{BG}} = 9$ and $V_{\mathrm{SG}} = -10.6$ V. The curves are shifted for clarity to the right by an offset of 2 V/T (200 mV between consecutive curves). The thicker black line (not shifted) corresponds to the data acquired at $B = 20$ mT, which is shown in Fig. 2. (b) Corresponding gray scale map of dG/dV_{TG} as a function of V_{TG} and B. Colored dashed lines at $B = 0.9$ (orange), 1.5 (blue), 2.2 (green), and 8.0 T (red) denote the line cuts associated with the highlighted conductance traces shown in (a). Transitions across magnetoelectric subbands appear as dark lines. (c) Energy level diagram of the QPC at zero and high magnetic field. (d) Valley subband dispersion as a function of B calculated with our model. The numbers displayed in the plot correspond to the quantized conductance values of the plateaus in units of e^2/h.

depicts schematically the pattern of energy levels in the QPC at zero and at high B, while Fig. 4(d) shows the evolution of the 1D subbands with magnetic field resulting from Eqs. (1) and (2). Comparing this plot with Fig. 4(b), we see that our simplified model captures the main qualitative features of the valley splitting induced by magnetic field. An additional splitting of Landau levels LL_1 and LL_2 observed in the experiment can be attributed to the renormalization (most prominent at the lowest densities) of the Zeeman splitting (neglected in our model) by the Coulomb interaction.

Finally, although we focused on the most clear conductance quantization in steps of $4e^2/h$ characteristic of a strong constriction, we mention that at smaller SG voltage, $V_{\mathrm{SG}} < -9.5$ V at $V_{\mathrm{BG}} = 9$ V, we observe a vanishing of the first plateau and a new $8e^2/h$ step in the quantization of the lowest subband appears [see Fig. 2(b)] The additional degeneracy is also apparent in the depopulation of the magnetoelectric subbands [51]. This is in agreement with the prediction of Ref. [40] about the possibility of "accidental" degeneracy of the size-quantized subbands in smoother constrictions that results from the Mexican-hat feature of the spectrum.

To conclude, we have studied the valley splitting in a BLG QPC subject to magnetic field. We have measured the quantized conductance through the QPC and observed robust and stable conductance steps quantized in units of $4e^2/h$, as expected for this fourfold degenerate system with a small band gap. Using source-drain bias spectroscopy, we have determined the 1D subband spacing $\Delta E_{N,N+1}$ which reveals an apparent unconventional confinement. Under high magnetic field B perpendicular to the sample plane, both spin and valley degeneracy fully lift as the density is lowered; i.e., as both confinement and Coulomb interactions are enhanced, magnetoelectric subbands are formed [47], reflecting the peculiar pseudospin structure of BLG. Our semiphenomenological model demonstrates that the QPC size-quantized modes undergo subband mixing and

merging of the K and K' valleys with nonconsecutive indices. Indeed, for higher modes, the conductance quantization in units of $4e^2/h$ is restored in strong magnetic fields. At the same time, for the lowest two resulting Landau levels, the Zeeman splitting is enhanced by interactions, leading to the observed steps of e^2/h in the conductance [red curve in Fig. 4(a)]. At intermediate fields, a complex pattern of the energy levels produces also the conductance steps of $2e^2/h$ due to valley splitting [orange and green curve in Fig. 4(a)], as well as the restored but shifted sequence $(N+1/2)4e^2/h$ when split lines from neighboring subbands are crossing [blue curve in Fig. 4(a)]. Our study thus demonstrates high versatility of band engineering in BLG and provides an input for developing graphene-based valleytronics.

This work was partly supported by Helmholtz society through program STN, the Russian Science Foundation (I. V. K., A. P. D., and I. V. G., Grant No. 17-12-01182, theoretical modeling), the Foundation for the Advancement of Theoretical Physics and Mathematics BASIS (I. V. K.), and the DFG via the Project No. DA 1280/3-1 and the FLAG-ERA JTC2017 Project GRANSPORT (GO 1405/5-1, Karlsruhe node).

Note added.—Recently we became aware of Ref. [62], which reported on the conductance quantization in a similar structure but with a top gate covering only the QPC region.

*Author to whom correspondence should be addressed.
romain.danneau@kit.edu

[1] B. J. van Wees, H. van Houten, C. W. J. Beenakker, J. G. Williamson, L. P. Kouwenhoven, D. van der Marel, and C. T. Foxon, Phys. Rev. Lett. **60**, 848 (1988).
[2] D. A. Wharam, T. J. Thornton, R. Newbury, M. Pepper, H. Ahmed, J. E. F. Frost, D. G. Hasko, D. C. Peacock, D. A. Ritchie, and G. A. C. Jones, J. Phys. C **21**, L209 (1988).
[3] C. W. J. Beenakker and H. van Houten, Solid State Phys. **44**, 1 (1991).
[4] H. van Houten, C. W. J. Beenakker, and B. J. van Wees, Semicond. Semimet. **35**, 9 (1992).
[5] S. Datta, *Electronic Transport in Mesoscopic Systems* (Cambridge University Press, Cambridge, 1995).
[6] T. J. Thornton, M. Pepper, H. Ahmed, D. Andrews, and G. J. Davies, Phys. Rev. Lett. **56**, 1198 (1986).
[7] T. Giamarchi, *Quantum Physics in One Dimension* (Clarendon Press, Oxford, 2003).
[8] M. Henny, S. Oberholzer, C. Strunk, T. Heinzel, K. Ensslin, M. Holland, and C. Schönenberger, Science **284**, 296 (1999).
[9] Y. Ji, Y. Chung, D. Sprinzak, M. Heiblum, D. Mahalu, and H. Shtrikman, Nature (London) **422**, 415 (2003).
[10] E. Bocquillon, V. Freulon, J.-M. Berroir, P. Degiovanni, B. Plaçais, A. Cavanna, Y. Jin, and G. Fève, Science **339**, 1054 (2013).
[11] M. Field, C. G. Smith, M. Pepper, D. A. Ritchie, J. E. F. Frost, G. A. C. Jones, and D. G. Hasko, Phys. Rev. Lett. **70**, 1311 (1993).
[12] D. Sprinzak, Y. Ji, M. Heiblum, D. Mahalu, and H. Shtrikman, Phys. Rev. Lett. **88**, 176805 (2002).
[13] L. M. K. Vandersypen, J. M. Elzerman, R. N. Schouten, L. H. Willems van Beveren, R. Hanson, and L. P. Kouwenhoven, Appl. Phys. Lett. **85**, 4394 (2004).
[14] S. Gustavsson, R. Leturcq, B. Simovic, R. Schleser, T. Ihn, P. Studerus, K. Ensslin, D. C. Driscoll, and A. C. Gossard, Phys. Rev. Lett. **96**, 076605 (2006).
[15] D. J. Reilly, C. M. Marcus, M. P. Hanson, and A. C. Gossard, Appl. Phys. Lett. **91**, 162101 (2007).
[16] M. C. Cassidy, A. S. Dzurak, R. G. Clark, K. D. Petersson, I. Farrer, D. A. Ritchie, and C. G. Smith, Appl. Phys. Lett. **91**, 222104 (2007).
[17] D. Többen, D. A. Wharam, G. Abstreiter, J. P. Kolthaus, and F. Schaffler, Semicond. Sci. Technol. **10**, 711 (1995).
[18] U. Wieser, U. Kunze, K. Ismail, and J. O. Chu, Appl. Phys. Lett. **81**, 1726 (2002).
[19] G. Scappucci, L. Di Gaspare, E. Giovine, A. Notargiacomo, R. Leoni, and F. Evangelisti, Phys. Rev. B **74**, 035321 (2006).
[20] S. Goswami, K. A. Slinker, M. Friesen, L. M. McGuire, J. L. Truitt, C. Tahan, L. J. Klein, J. O. Chu, P. M. Moonney, D. W. van Derweide, R. Joynt, S. N. Coppersmith, and M. A. Eriksson, Nat. Phys. **3**, 41 (2007).
[21] L. M. McGuire, M. Friesen, K. A. Slinker, S. N. Coppersmith, and M. A. Eriksson, New J. Phys. **12**, 033039 (2010).
[22] O. Gunawan, B. Habib, E. P. De Poortere, and M. Shayegan, Phys. Rev. B **74**, 155436 (2006).
[23] M. J. Biercuk, N. Mason, J. Martin, A. Yacoby, and C. M. Marcus, Phys. Rev. Lett. **94**, 026801 (2005).
[24] Y.-M. Lin, V. Perebeinos, Z. Chen, and P. Avouris, Phys. Rev. B **78**, 161409(R) (2008).
[25] C. Lian, K. Tahy, T. Fang, G. Li, H. G. Xing, and D. Jenaa, Appl. Phys. Lett. **96**, 103109 (2010).
[26] N. Tombros, A. Veligura, J. Junesch, M. H. D. Guimarães, I. J. Vera-Marun, H. T. Jonkman, and B. J. van Wees, Nat. Phys. **7**, 697 (2011).
[27] M. T. Allen, J. Martin, and A. Yacoby, Nat. Commun. **3**, 934 (2012).
[28] A. M. Goossens, S. C. M. Driessen, T. A. Baart, K. Watanabe, T. Taniguchi, and L. M. K. Vandersypen, Nano Lett. **12**, 4656 (2012).
[29] S. Dröscher, C. Barraud, K. Watanabe, T. Taniguchi, T. Ihn, and K. Ensslin, New J. Phys. **14**, 103007 (2012).
[30] B. Terrés, L. A. Chizhova, F. Libisch, J. Peiro, D. Jörger, S. Engels, A. Girschik, K. Watanabe, T. Taniguchi, S. V. Rotkin, C. Burgdörfer, and C. Stampfer, Nat. Commun. **7**, 11528 (2016).
[31] J. Li, K. Wang, K. J. McFaul, Z. Zern, Y. Ren, K. Watanabe, T. Taniguchi, Z. Qiao, and J. Zhu, Nat. Nanotechnol. **11**, 1060 (2016).
[32] S. Somanchi, B. Terrés, J. Peiro, M. Staggenborg, K. Watanabe, T. Taniguchi, B. Beschoten, and C. Stampfer, Ann. Phys. (Berlin) **529**, 1700082 (2017).
[33] H. Overweg, H. Eggimann, X. Chen, S. Slizovskiy, M. Eich, R. Pisoni, Y. Lee, P. Rickhaus, K. Watanabe, T. Taniguchi, V. Fal'ko, T. Ihn, and K. Ensslin, Nano Lett. **18**, 553 (2018).

[34] J. M. Caridad, S. R. Power, M. R. Lotz, A. A. Shylau, J. D. Thomsen, L. Gammelgaard, T. J. Booth, A.-P. Jauho, and P. Bøggild, Nat. Commun. **9**, 659 (2018).
[35] L. Banszerus, B. Frohn, A. Epping, D. Neumaier, K. Watanabe, T. Taniguchi, and C. Stampfer, Nano Lett. **18**, 4785 (2018).
[36] J. R. Schaibley, H. Yu, G. Clark, P. Rivera, J. S. Ross, K. L. Seyler, W. Yao, and X. Xu, Nat. Rev. Mater. **1**, 16055 (2016).
[37] P. Recher, B. Trauzettel, A. Rycerz, Ya. M. Blanter, C. W. J. Beenakker, and A. F. Morpurgo, Phys. Rev. B **76**, 235404 (2007).
[38] P. Recher, J. Nilsson, G. Burkard, and B. Trauzettel, Phys. Rev. B **79**, 085407 (2009).
[39] L. M. Zhang, M. M. Fogler, and D. P. Arovas, Phys. Rev. B **84**, 075451 (2011).
[40] A. Knothe and V. Fal'ko, Phys. Rev. B **98**, 155435 (2018).
[41] A. Rycerz, J. Tworzydło, and C. W. J. Beenakker, Nat. Phys. **3**, 172 (2007).
[42] B. Trauzettel, D. V. Bulaev, D. Loss, and G. Burkard, Nat. Phys. **3**, 192 (2007).
[43] R. Kraft, J. Mohrmann, R. Du, P. B. Selvasundaram, M. Irfan, U. N. Kanilmaz, F. Wu, D. Beckmann, H. von Löhneysen, R. Krupke, A. Akhmerov, I. Gornyi, and R. Danneau, Nat. Commun. **9**, 1722 (2018).
[44] N. K. Patel, L. Martin-Moreno, M. Pepper, R. Newbury, J. E. F. Frost, D. A. Ritchie, G. A. C. Jones, J. T. M. B. Janssen, J. Singleton, and J. A. A. J. Perenboom, J. Phys. Condens. Matter **2**, 7247 (1990).
[45] N. K. Patel, J. T. Nicholls, L. Martin-Moreno, M. Pepper, J. E. F. Frost, D. A. Ritchie, and G. A. C. Jones, Phys. Rev. B **44**, 13549 (1991).
[46] L. Martin-Moreno, J. T. Nicholls, N. K. Patel, and M. Pepper, J. Phys. Condens. Matter **4**, 1323 (1992).
[47] B. J. van Wees, L. P. Kouwenhoven, H. van Houten, C. W. J. Beenakker, J. E. Mooij, C. T. Foxon, and J. J. Harris, Phys. Rev. B **38**, 3625 (1988).
[48] L. I. Glazman and A. V. Khaetskii, Europhys. Lett. **9**, 263 (1989).
[49] E. McCann, Phys. Rev. B **74**, 161403 (2006).
[50] E. McCann and M. Koshino, Rep. Prog. Phys. **76**, 056503 (2013).
[51] See Supplemental Material at http://link.aps.org/supplemental/10.1103/PhysRevLett.121.257703 for details of device fabrication and measurement, additional data, and methods of the analysis, which includes Refs. [52–54].
[52] L. Wang, I. Meric, P. Y. Huang, Q. Gao, Y. Gao, H. Tran, T. Taniguchi, K. Watanabe, L. M. Campos, D. A. Muller, J. Guo, P. Kim, J. Hone, K. L. Shepard, and C. R. Dean, Science **342**, 614 (2013).
[53] E. McCann and V. I. Falko, Phys. Rev. Lett. **96**, 086805 (2006).
[54] J. B. Oostinga, H. B. Heersche, X. Liu, A. F. Morpurgo, and L. M. K. Vandersypen, Nat. Mater. **7**, 151 (2008).
[55] K. S. Pyshkin, C. J. B. Ford, R. H. Harrell, M. Pepper, E. H. Linfield, and D. A. Ritchie, Phys. Rev. B **62**, 15842 (2000).
[56] W. K. Hew, K. J. Thomas, M. Pepper, I. Farrer, D. Anderson, G. A. C. Jones, and D. A. Ritchie, Phys. Rev. Lett. **101**, 036801 (2008).
[57] W. K. Hew, K. J. Thomas, M. Pepper, I. Farrer, D. Anderson, G. A. C. Jones, and D. A. Ritchie, Phys. Rev. Lett. **102**, 056804 (2009).
[58] Here, the contact resistance was estimated on the order of $\sim$115 $\Omega\mu$m at large density, i.e., small compared to the 1D constriction resistance. Therefore, we have decided not to substract any contact resistance.
[59] K. J. Thomas, J. T. Nicholls, M. Y. Simmons, M. Pepper, D. R. Mace, and D. A. Ritchie, Phys. Rev. Lett. **77**, 135 (1996).
[60] A. P. Micolich, J. Phys. Condens. Matter **23**, 443201 (2011).
[61] K. Zimmermann, A. Jordan, F. Gay, K. Watanabe, T. Taniguchi, Z. Han, V. Bouchiat, H. Sellier, and B. Sacépé, Nat. Commun. **8**, 14983 (2017).
[62] H. Overweg *et al.*, preceding Letter, Phys. Rev. Lett. **121**, 257702 (2018).